AIAA 01-2572

The Development of a Factorizable Multigrid Algorithm for Subsonic and Transonic Flow

Thomas W. Roberts

NASA Langley Research Center

Hampton, VA

15th AIAA Computational Fluid Dynamics Conference

11–14 June 2001/Anaheim, CA

THE DEVELOPMENT OF A FACTORIZABLE MULTIGRID ALGORITHM FOR SUBSONIC AND TRANSONIC FLOW

Thomas W. Roberts*
NASA Langley Research Center
Hampton, VA

Abstract

The factorizable discretization of Sidilkover for the compressible Euler equations previously demonstrated for channel flows has been extended to external flows. The dissipation of the original scheme has been modified to maintain stability for moderately stretched grids. The discrete equations are solved by symmetric collective Gauss-Seidel relaxation and FAS multigrid. Unlike the earlier work, ordering the grid vertices in the flow direction has been found to be unnecessary. Solutions for essential incompressible flow (Mach 0.01) and supercritical flows have been obtained for a Kármán-Trefftz airfoil with a conformally mapped grid, as well as a NACA 0012 on an algebraically generated grid. The current work demonstrates nearly $O(n)$ convergence for subsonic and slightly transonic flows.

Introduction

In the past several years, there has been an ongoing effort in the Computational Modeling and Simulation Branch of NASA Langley Research Center, in collaboration with researchers at ICASE, to develop algorithms demonstrating "Textbook Multigrid Efficiency" (TME)[1, 2, 3]. The central theme of this effort has been the idea of Brandt[4] that ideal convergence rates for the numerical solution of partial differential equations can be achieved if the relaxation scheme distinguishes between elliptic, parabolic, and hyperbolic partitions of the differential operator. Construction of an ideally converging method requires that each of these partitions be treated independently and optimally. To achieve this, efforts are being made to construct so-called "factorizable" difference schemes for the equations of fluid dynamics. A factorizable scheme is one in which the discretization correctly separates the elliptic, parabolic, and hyperbolic partitions.

In the case of steady inviscid flow, the Euler equations can be considered as a composition of two subsystems. One subsystem corresponds to the equations governing entropy and vorticity advection. This subsystem is hyperbolic in space. The other subsystem corresponds to a full potential operator, which is elliptic for subsonic flow and hyperbolic for supersonic flow. For a purely supersonic flow, space marching is the most efficient way of solving the Euler equations. For subsonic flow, the ellipticity of the full potential factor should be effectively handled by multigrid. However multigrid is not effective for advection operators, as the coarse grid only gives part of the correction for certain smooth components of the error. Existing multigrid methods for subsonic and transonic flow rely on the coarse grid to smooth the entire system. As such, they are fundamentally limited by the ineffectiveness of the coarse grid in correcting the part of the error corresponding to advection factor. This same difficulty is true for high Reynolds number viscous flows.

Sidilkover[5] has devised a Cartesian grid discretization of the Euler equations that separates these two subsystems. In a previous work, Roberts, Sidilkover and Thomas[3] extended this scheme in conservation form to general body-fitted curvilinear coordinates. Solutions to the equations were obtained using collective point Gauss-Seidel relaxation as a smoother combined with FAS multigrid. Results for subsonic and transonic channel flows were presented in Ref. 3, which demonstrated essentially grid independent convergence rates. All the grids used for these cases were quasi-uniform, with grid cells of unit aspect ratio. Furthermore, the channel wall had a continuous curvature to preclude the presence of stagnation points, and the relaxation sweep was made in the flow direction.

In the present paper, the work of Roberts, et al.[3] is extended to external lifting flows around airfoils with both subcritical and supercritical freestream Mach numbers. The presence of a stagnation point at the airfoil leading edge requires an additional dissipation term in the momentum equation. The form of this dissipation was presented in Ref. 3 and is found to be effective. Computations are shown in which an odd-even vorticity error is propagated downstream of the airfoil. This error originates at the trailing edge of the airfoil, and causes erratic convergence. A dissipation term to smooth this vortical error is added to the momentum equations.

The mathematical formulation of the scheme, which has been presented by Sidilkover[5] and Roberts, et al.[3] is briefly recounted in the following section. Modifications to the scheme as presented in Ref. 3 are noted. Follow-

* Research Scientist

ing that, the multigrid relaxation is described. Subsonic channel flow results are presented to demonstrate the second-order convergence of the discretization. Results for subsonic and transonic airfoils are presented next. Subsonic solutions for a Kármán-Trefftz airfoil are used to compare with an exact solution. In addition, a transonic solution for this airfoil is presented. The Kármán-Trefftz airfoil airfoil uses a conformally-mapped grid with unit aspect ratio cells. To demonstrate the effectiveness of the scheme when applied to a more realistic case, subsonic and transonic flow around a NACA 0012 is also presented. These computations are performed on a grid generated algebraically, with moderate grid stretching, skewness, and aspect ratio.

Mathematical Formulation

The artificial dissipation of the factorizable scheme can be described by first presenting the modified equation, or first differential approximation (FDA), of the discrete scheme. This is the differential equation which is found by expanding the difference equation in a Taylor series about each grid vertex and considering the leading terms of the truncation error. These terms are the artificial dissipation of the scheme.

The starting point for the scheme is the two-dimensional Euler equations in non-conservation form. Let ρ be the density, $\vec{u} = \hat{\imath}u + \hat{\jmath}v$ be the velocity, and p be the pressure. The entropy s is defined as

$$s \equiv \left(\frac{p}{p_0}\right)\left(\frac{\rho}{\rho_0}\right)^{-\gamma}, \tag{1}$$

where p_0 and ρ_0 are a reference pressure and density, respectively, and γ is the ratio of the specific heats. Then the Euler equations may be written in the variables (s, u, v, p):

$$\vec{u}\cdot\nabla s = 0, \tag{2a}$$

$$\vec{u}\cdot\nabla\vec{u} + \frac{1}{\rho}\nabla p = 0, \tag{2b}$$

$$\rho c^2\nabla\cdot\vec{u} + \vec{u}\cdot\nabla p = 0. \tag{2c}$$

The factorizability of the scheme depends on the form of the artificial dissipation added to this system of equations.

The entropy is only weakly coupled to the momentum and the pressure equations through the equation of state (1). In fact, the entropy equation corresponds to one of the advection factors of the Euler equations. Therefore, it may be discretized independently of the momentum and pressure equations in any appropriate way without affecting the factorizability of the scheme. The advection operator $\vec{u}\cdot\nabla$ uses simple upwind differencing in Eq. (2a). Let (ξ, η) be a general curvilinear coordinate system and define the contravariant components of the velocity, (U, V) by the transformation

$$\begin{pmatrix} x_\xi & x_\eta \\ y_\xi & y_\eta \end{pmatrix}\begin{pmatrix} U \\ V \end{pmatrix} = \begin{pmatrix} u \\ v \end{pmatrix}. \tag{3}$$

In this coordinate system $\vec{u}\cdot\nabla\vec{u} = U\partial_\xi + V\partial_\eta$. The equations are discretized on a uniform grid in (ξ, η) space, with a grid spacing $\Delta\xi = \Delta\eta = 1$. The FDA of the first-order upwind difference approximation to $\vec{u}\cdot\nabla$ is

$$\mathbf{q} \equiv \vec{u}\cdot\nabla - \frac{1}{2}\left|U\right|\partial_\xi^2 - \frac{1}{2}\left|V\right|\partial_\eta^2 = 0, \tag{4}$$

and the entropy equation is discretized as

$$\mathbf{q}s = 0. \tag{5}$$

A second-order upwind discretization of the advection operator has also been used in Eq. (5). However, it was shown in Ref. 3 that the use of a second-order advection operator has an insignificant affect on the computed results.

The dissipation for the momentum and pressure equations, Eqs. (2b) and (2c) given in Ref. 3 is the multidimensional upwind dissipation of Sidilkover[6]. In vector notation, this dissipation is written as

$$\vec{u}\cdot\nabla\vec{u} + \frac{1}{\rho}\nabla p - \frac{\sigma_m\ell}{2\rho c}\nabla\left(\rho c^2\nabla\cdot\vec{u} + \vec{u}\cdot\nabla p\right) = 0, \tag{6}$$

$$\rho c^2\nabla\cdot\vec{u} + \vec{u}\cdot\nabla p - \rho c\frac{\sigma_p\ell}{2}\nabla\cdot\left(\vec{u}\cdot\nabla\vec{u} + \frac{1}{\rho}\nabla p\right) = 0, \tag{7}$$

where c is the speed of sound, σ_m and σ_p are scaling coefficients, and ℓ is a length scale proportional to the grid spacing. Note that the dissipation of the momentum equation is the gradient of the pressure equation residual, and the dissipation of the pressure equation is the divergence of the momentum equation residual. Also note that the curl of Eq. (6) is identical to the curl of Eq. (2b), i.e., vorticity equation of the governing Euler equations is unaffected by the artificial dissipation. The vorticity equation corresponds to the second advection factor of the Euler equations.

If the advection operator, pressure gradient, and divergence term in Eqs. (6) and (7) are discretized using central differences, the scheme is second-order accurate and factorizable. However, such a scheme is not h-elliptic. This lack of h-ellipticity is a result of the central difference approximation to the advection term in the momentum equation, Eq. (6). Sidilkover shows that this advection operator corresponds to vorticity advection[5]. Replacing this operator by the first-order upwind approximation in Eq. (4) restores h-ellipticity and the scheme remains factorizable, but it now becomes only first-order accurate. Note that the pressure advection term in Eq. (7) continues to be approximated by second-order central differences.

To obtain second-order accuracy while maintaining h-ellipticity, the advection operator in the momentum equation must be replaced with an upwind difference operator. However, this operator also contributes to the full potential operator. Simply replacing the central difference with an upwind difference will change the form of the full potential operator, which we wish to avoid. To

obtain a second-order upwind advection operator without changing the full potential operator, Eq. (6) is modified to be

$$\vec{u}\cdot\nabla\vec{u} + \frac{1}{\rho}\nabla p + \frac{\ell}{2q}\vec{u}\times\nabla\times\left(\vec{u}\cdot\nabla\vec{u} + \frac{1}{\rho}\nabla p\right) - \frac{\sigma_m \ell}{2\rho c}\nabla\left(\rho c^2\nabla\cdot\vec{u} + \vec{u}\cdot\nabla p\right) = 0. \quad (8)$$

where $q = \max(|u|,|v|)$. Because the additional term involves the curl of the momentum equation, it is transparent to irrotational disturbances. If a solution is a pure potential solution, then not only is Eq. (6) satisfied identically, but Eq. (8) is satisfied as well. Because the continuity equation (7) is unchanged, a potential solution to Eq. (6) and (7) is a solution to Eq. (8) and (7). In other words, the modification to the momentum equation does not change the full potential operator, which is what is wanted.

Expanding the additional term in Eq. (8) the principal part of the operator is

$$\frac{\ell}{2q}\vec{u}\times\nabla\times\left(\vec{u}\cdot\nabla\vec{u} + \frac{1}{\rho}\nabla p\right) = \frac{\ell}{2q}\left[-(\vec{u}\cdot\nabla)^2\vec{u} + \nabla\left(\vec{u}\cdot\nabla\frac{u^2+v^2}{2}\right) + \vec{u}\times\nabla\frac{1}{\rho}\times\nabla p\right]. \quad (9)$$

The first term in the square brackets may be combined with the advection operator in Eq. (8) to yield the FDA of a second-order upwind advection operator. This second-order operator operator is denoted as $\mathbf{q}_{\mathrm{HO}}$. The pressure terms can be manipulated such that the remaining terms in the square brackets be can be written in the form ∇D. This puts the momentum equation in the form

$$\mathbf{q}_{\mathrm{HO}}\vec{u} + \nabla D + \frac{1}{\rho}\nabla p - \frac{\sigma_m \ell}{2\rho c}\nabla\left(\rho c^2\nabla\cdot\vec{u} + \vec{u}\cdot\nabla p\right) = 0. \quad (10)$$

In Roberts, et al.[3] the pressure term in Eq. (9) was ignored because the principal part of this term vanishes. In fact, if the flow is barotropic the term vanishes identically. However, failure to include this term in the conservative discretization gives rise to a first order error, a point that was not recognized at the time. In the current work these terms are included in the discretization.

Discretization

The factorizability of the FDA is a necessary condition for the factorizability of the difference scheme, but it is not sufficient. For the difference scheme to be factorizable, the difference operators must commute in the same way as the differential operators[5]. Introducing the difference approximations to the partial derivative operators,

$$\partial_\xi^h = \partial_\xi + \cdots, \qquad \partial_\eta^h = \partial_\eta + \cdots,$$
$$\partial_{\xi\xi}^h = \partial_\xi^2 + \cdots, \qquad \partial_{\eta\eta}^h = \partial_\eta^2 + \cdots,$$
$$\partial_{\xi\eta}^h = \partial_\xi\partial_\eta + \cdots,$$

the following conditions must hold

$$\partial_{\xi\xi}^h\partial_{\eta\eta}^h = \partial_{\xi\eta}^h\partial_{\xi\eta}^h$$
$$\partial_{\xi\xi}^h\partial_\eta^h = \partial_{\xi\eta}^h\partial_\xi^h,$$
$$\partial_{\eta\eta}^h\partial_\xi^h = \partial_{\xi\eta}^h\partial_\eta^h.$$

The following difference operators satisfy this condition:

$$\partial_\xi^h = \frac{1}{8}\begin{bmatrix}-1 & 0 & 1\\ -2 & 0 & 2\\ -1 & 0 & 1\end{bmatrix}, \quad \partial_\eta^h = \frac{1}{8}\begin{bmatrix}1 & 2 & 1\\ 0 & 0 & 0\\ -1 & -2 & -1\end{bmatrix},$$
$$\partial_{\xi\xi}^h = \frac{1}{4}\begin{bmatrix}1 & -2 & 1\\ 2 & -4 & 2\\ 1 & -2 & 1\end{bmatrix}, \quad \partial_{\eta\eta}^h = \frac{1}{4}\begin{bmatrix}1 & 2 & 1\\ -2 & -4 & -2\\ 1 & 2 & 1\end{bmatrix},$$
$$\partial_{\xi\eta}^h = \frac{1}{4}\begin{bmatrix}-1 & 0 & 1\\ 0 & 0 & 0\\ 1 & 0 & -1\end{bmatrix}.$$

To write the complete discrete scheme, the subscript h is used to denote a standard difference to the corresponding operator, and the addition of the overbar ( ) denotes the "wide" differences given above. The second-difference expressions may be expressed in flux form by taking a six-point difference centered on an edge between two vertices, and then taking a two-point difference of those expressions centered on a vertex. The subscripts e and v are used to denote difference operators centered on an edge or a vertex, respectively. The fully discrete scheme is then written as

$$\mathbf{q}^h s = 0. \quad (11a)$$

$$\mathbf{q}_{\mathrm{HO}}^h\vec{u} + \nabla_v D^h + \frac{1}{\rho}\nabla^h p - \frac{\sigma_m \ell}{2\rho c}\nabla_v^h\left(\rho c^2\nabla_v^h\cdot\vec{u} + \vec{u}\cdot\nabla_v^h p\right) = 0. \quad (11b)$$

$$\rho c^2\nabla^h\cdot\vec{u} + \vec{u}\cdot\nabla^h p - \rho c\frac{\sigma_p}{2}\nabla_v^h\cdot\left(\vec{u}\cdot\nabla_v^h\vec{u} + \frac{1}{2\rho}\left(\nabla_e^h + \nabla_v^h\right)p\right) = 0. \quad (11c)$$

Details of the velocity terms in D are found in the Ref. 3. The pressure terms in D are evaluated using the wide difference operators defined above.
The scaling coefficients are

$$\sigma_m = \max(M, M_c), \qquad \sigma_p = \frac{1}{\max(M, M_c)} \quad (12)$$

where M is the local Mach number, and M_c is a cutoff Mach number to prevent division by zero. The cutoff is chosen to be $O(h)$, and essentially becomes active near stagnation points. The purpose of the rescaling of the pressure equation dissipation, σ_p, is to prevent the elliptic factor in the discrete equations from becoming the skewed Laplacian operator in the incompressible limit.

Currently, we take $M_c = \nu|\Delta M|$, where $\nu = 2$ and ΔM is the two-point difference in Mach number on an edge. When $M_c > M$, it is necessary to add additional dissipation to the advection operator $\mathbf{q}^h$. The form of this dissipation is a five-point pseudo-Laplacian,

$$d_{\rm sp}\vec{u} = \frac{1}{2}\max(0, M_c - M)\frac{c\ell}{J}\left(\partial_\xi^2 + \partial_\eta^2\right)\vec{u}, \qquad (13)$$

where J is the Jacobian of the coordinate transformation, $J \equiv x_\xi y_\eta - y_\xi x_\eta$. This operator is added to both the entropy and the momentum equation, and is cast in flux form in order to maintain conservation. No attempt has been made to optimize either the coefficient ν or the form of the operator $d_{\rm sp}$.

When solving for the flow around an airfoil, it has been observed that a short-wavelength vorticity error is generated near the trailing edge and is propagated downstream. This error is an odd-even error of the streamwise velocity component in the crossflow direction. The error persists to the outflow boundary, and can cause convergence difficulties. An additional dissipative term must be added to the momentum equation to reduce the error. Care must be taken to insure that the dissipation does not affect the factorizability of the scheme and preserves second-order accuracy.

The form of this dissipation follows from a formulation of Giles[7], who observed that $\nabla \times \vec{\omega} = \nabla(\nabla\cdot\vec{u}) - \nabla^2\vec{u}$. The Laplacian acting on $\vec{u}$ is dissipative. In the present scheme, the addition of a term of this form to the momentum equation will not affect the factorizability of the scheme, as it is transparent to the irrotational, potential part of the solution. This vorticity dissipation is

$$d_{\rm v}\vec{u} = \mu\left|\ell\hat{k}\times\Delta\vec{u}\right|\nabla_v^h\times\vec{\omega}_v^h, \qquad (14)$$

where μ is a dissipation coefficient, $\Delta\vec{u}$ is an undivided difference of the velocity in a grid direction, ℓ is the grid spacing directed in that direction, and $\vec{\omega}_v^h$ is the discrete vorticity centered on an edge and computed using the wide differences. Currently the coefficient μ is taken to be 0.1. No attempt has been made to optimize this dissipation.

As written, the Eq. (11) is valid only for subsonic flows. This is because the pressure differences in the artificial dissipation terms are not fully upwinded in a supersonic zone. A simple modification to Eq. (11) can be made by rescaling the gradients of the pressure when the flow becomes sonic. Introducing the parameter κ, defined as

$$\kappa = \max(1, M^2), \qquad (15)$$

the final form of the scheme is

$$\mathbf{q}^h s - d_{\rm sp}s = 0, \qquad (16a)$$

$$\mathbf{q}_{\rm HO}^h\vec{u} - d_{\rm sp}\vec{u} + d_{\rm v}\vec{u} + \nabla_v D^h + \frac{1}{\rho}\nabla^h p - \frac{\sigma_m\ell}{2\rho c}\nabla_v^h\left(\rho c^2\bar{\nabla}_v^h\cdot\vec{u} + \frac{1}{\kappa}\vec{u}\cdot\nabla_v^h p\right) = 0, \qquad (16b)$$

$$\rho c^2\nabla^h\cdot\vec{u} + \vec{u}\cdot\nabla^h p - \rho c\frac{\sigma_p}{2}\nabla_v^h\cdot\left(\vec{u}\cdot\nabla_v^h\vec{u} + \frac{\kappa}{2\rho}\left(\nabla_v^h + \nabla_v^h\right)p\right) = 0. \qquad (16c)$$

Because the difference equations (16a), (16b) and (16c), can be written as a central difference part plus a dissipation, it is straightforward to obtain a conservative discretization. The conservation form of the Euler equations are discretized using a central-difference finite-volume approximation,

$$\nabla^h\cdot(\rho\vec{u}) = 0, \qquad (17a)$$

$$\nabla^h\cdot(\rho\vec{u}\vec{u}) + \nabla^h p = 0, \qquad (17b)$$

$$\nabla^h\cdot[(\rho e + p)\vec{u}] = 0 \qquad (17c)$$

where $e = \vec{u}\cdot\vec{u}/2 + p/(\rho(\gamma - 1))$ is the total energy. The dissipative fluxes on each cell face are computed in terms of (s, u, v, p) using the appropriate difference operators in Eq. (16). The artificial dissipation in Eqs. (16b) and (16c) can be rewritten as

$$\delta\vec{u} = -\nabla_v D^h + d_{\rm sp}\vec{u} - d_{\rm v}\vec{u} + \nabla_v^h\left[\frac{\sigma_m\ell}{2}\left(c\nabla_v^h\cdot\vec{u} + \frac{1}{\rho c\kappa}\vec{u}\cdot\nabla_v^h p\right)\right]. \qquad (18)$$

$$\delta p = \nabla_v^h\cdot\left[\frac{\sigma_p}{2}\left(\rho c\vec{u}\cdot\nabla^h\vec{u} + \frac{c\kappa}{2}\left(\nabla_v^h + \bar{\nabla}_v^h\right)p\right)\right]. \qquad (19)$$

This is a conservative form of the dissipation cast in terms of the primitive variables. The terms inside the square bracket in Eqs. (18) and (19) are now interpreted as dissipative fluxes. These terms are discretized on cell faces according to the appropriate wide or narrow differences. The first and second-order upwind advection operators $\mathbf{q}^h$ and $\mathbf{q}_{\rm HO}^h$ and the terms $\nabla_v D^h$ in Eq. (18) may be recast in conservation form and evaluated on cell faces. The length scale ℓ is evaluated on the cell face and is taken as either k_ξ or k_η is used, whichever is more nearly aligned with the flow direction. This assures that the advection operator in Eq. (16b) is fully upwinded when the flow is grid-aligned. The scaling coefficients σ_m and σ_p are evaluated using the Mach number on the face.

In addition to the dissipation terms, examination of Eqs. (16b) and (16c) shows that the pressure gradient terms are discretized using the wide stencils. The central-difference part of the conservation equations (17) must be corrected to account for these wide differences. This is done by adding a term to the dissipative fluxes for the momentum and pressure equations as follows:

$$\delta\vec{u} \leftarrow \delta\vec{u} - \frac{1}{\rho}\left(\bar{\nabla}^h - \nabla^h\right)p, \qquad (20)$$

$$\delta p \leftarrow \delta p - \vec{u}\cdot\left(\bar{\nabla}^h - \nabla^h\right)p. \qquad (21)$$

Once the dissipative fluxes $(\delta s, \delta u, \delta v, \delta p)$ have been evaluated, they are converted to the conservation variables

by the transformation

$$\begin{pmatrix} \delta\rho \\ \delta\rho u \\ \delta\rho v \\ \delta\rho e \end{pmatrix} = \begin{pmatrix} -\rho/s & 0 & 0 & 1/c^2 \\ -\rho u/s & \rho & 0 & u/c^2 \\ -\rho v/s & 0 & \rho & v/c^2 \\ -\rho(u^2+v^2)/2s & \rho u & \rho v & h/c^2 \end{pmatrix} \begin{pmatrix} \delta s \\ \delta u \\ \delta v \\ \delta p \end{pmatrix}, \tag{22}$$

where $h = e + p/\rho$ is the total enthalpy.

Solution Procedure

The solution of the discrete equations is performed using a symmetric point collective Gauss-Seidel iteration, which has been found to be a very effective smoother. In the previous work[3] the grid vertices were ordered in the flow direction, so that the advection factor would be solved by marching during the forward sweep. Similarly, in the present work the grid vertices are sorted in the freestream direction. Each Gauss-Seidel sweep is underrelaxed with a factor of 0.7 for stability. The residuals of the conservation equations $(r_\rho, r_{\rho u}, r_{\rho v}, r_{\rho e})$ are computed at each vertex using the discretization presented in the previous section. These residuals are then transformed to the residuals of the primitive variables by the inverse of the transformation in Eq. (22).

At each point, the update to the solution is given by

$$\mathbf{M} \begin{pmatrix} \Delta s \\ \Delta u \\ \Delta v \\ \Delta p \end{pmatrix}_{i,j} = - \begin{pmatrix} r_s \\ r_u \\ r_v \\ r_p \end{pmatrix}_{i,j} \tag{23}$$

where $\mathbf{M}$ is the matrix of coefficients of the primitive variables at vertex (i, j). The coefficients are found by collecting the contributions to vertex (i, j) from the dissipation terms on the four surrounding faces. Because the entropy equation decouples from the rest of the system, this is a block diagonal matrix where the upper block is the upper left-hand entry, and the lower block is a 3×3 matrix of coefficients multiplying $u_{i,j}$, $v_{i,j}$, and $p_{i,j}$. This matrix is easily inverted.

The relaxation is accelerated using a standard Full-Approximation Scheme (FAS) multigrid. A sequence of grids $G_K, G_{K-1}, \ldots, G_0$ is used, where G_K is the finest and G_0 the coarsest. Let $\hat{\mathbf{L}}_{k-1}$ be the coarse grid operator, $\mathbf{u}$ be the vector of the conservation variables, I_{k-1}^k be the fine-to-coarse grid restriction operator, and I_k^{k-1} be the coarse-to-fine grid prolongation operator. If $\hat{\mathbf{u}}_k$ is the current solution on grid k, the residual on this grid is $\mathbf{r}_k \equiv \mathbf{f}_k - \hat{\mathbf{L}}_k \hat{\mathbf{u}}_k$. This is the residual of the conservation equations, not the primitive equations. This leads to the coarse-grid equation

$$\hat{\mathbf{L}}_{k-1}\hat{\mathbf{u}}_{k-1} = \mathbf{f}_{k-1} = I_{k-1}^k \mathbf{r}_k + \hat{\mathbf{L}}_{k-1}\left(I_{k-1}^k \hat{\mathbf{u}}_k\right). \tag{24}$$

After solving the coarse-grid equation for $\mathbf{u}_{k-1}$, the fine-grid solution is corrected by

$$\hat{\mathbf{u}}_k^{\text{new}} \leftarrow \hat{\mathbf{u}}_k + I_k^{k-1}\left(\hat{\mathbf{u}}_{k-1} - I_{k-1}^k \hat{\mathbf{u}}_k\right). \tag{25}$$

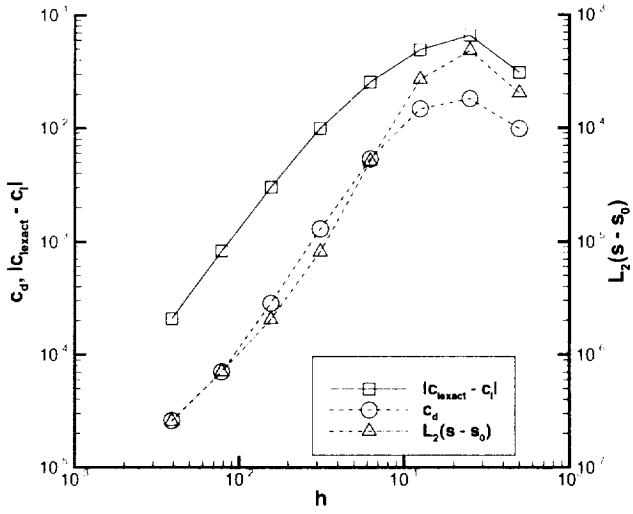

Figure 1. Convergence of lift, drag, and entropy for channel flow with a 10% bump on the lower wall

Equation (24) is solved by applying the same relaxation procedure that is used to solve the fine-grid equation. Multigrid is applied recursively to the coarse-grid equation. On the coarsest grid, many relaxation sweeps are performed to insure that the equation is solved completely. A conventional V-cycle or W-cycle is used.

Results

To confirm the order of accuracy of the scheme, solutions for the channel configuration used in Ref. 3 were obtained for a sequence of grids starting at 7×3 and ending at 769×257. Results are shown in Fig. 1. The lift and drag values are the integrated forces on the lower wall. Richardson extrapolation was used to compute the exact lift coefficient. The L_2 norm of the difference between the local and freestream entropy is also shown. It is seen that all three quantities exhibit second-order convergence in the grid spacing.

The first set of external flow results are for flow around a symmetric Kármán-Trefftz airfoil with a thickness ratio of about 0.15. An O-grid was generated using a conformal mapping and is shown in Fig. 2. The radial stretching factor was chosen to maintain unit cell aspect ratio, and grid lines are orthogonal. The finest grid for all cases is 257×257 and the coarsest grid is 5×5. The outer boundary is approximately 150 chord lengths from the airfoil.

Dirichlet conditions are used at the outer boundary, a uniform freestream being specified. No far-field vortex correction is applied. One-sided first-order differences are used at the wall. The tangency condition $\vec{u} \cdot \hat{n} = 0$ is enforced explicitly by zeroing-out the component of the momentum equation residual in the direction normal to

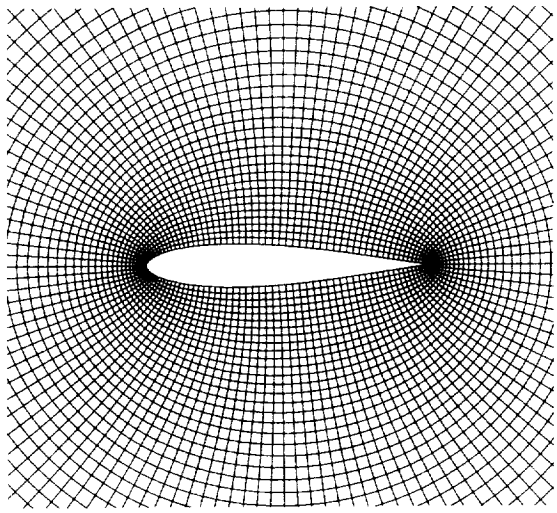

Figure 2. Conformal grid for Kármán-Trefftz airfoil.

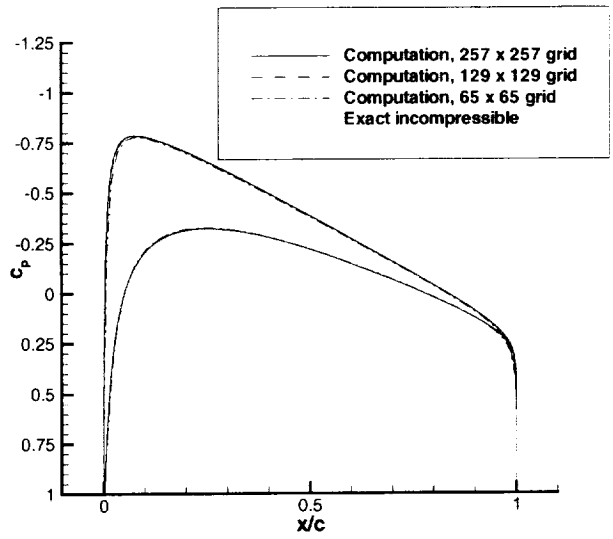

Figure 3. Surface C_p comparisons for a Kármán-Trefftz airfoil, $M_\infty = 0.01$, $\alpha = 2°$, finest grid 257×257 grid.

the wall.

Solutions are obtained using a FMG cycle to initialize the solution. A solution is computed on the coarsest grid and prolonged to the next grid to obtain a starting solution for that grid. This procedure is continued recursively until the finest grid is reached. On each grid, a $V(1,1)$ multigrid cycle is used to solve the system. Ten multigrid cycles are run on each of the coarse grids, and twenty cycles are run on the finest grid. After each symmetric Gauss-Seidel relaxation sweep, an additional six streamwise sweeps are done on the wall and its neighboring row of vertices.

For the first case the freestream Mach number is 0.01 and the angle-of-attack is 2°. A comparison of the computed surface pressure coefficient with the exact incompressible solution is shown in Fig. 3. Excellent agreement is seen. Convergence rates for the continuity equation residual as well as the lift and drag coefficients are shown in Fig. 4. On the coarse grids up to the 129×129 grid the convergence rate is essentially independent of the grid spacing, with an asymptotic rate of about 0.25. This slows down considerably on the 257×257 grid which has an asymptotic rate for the continuity residual of approximately 0.6 per cycle. There is some slightly erratic behavior in the convergence rate on the finest grid. Both lift and drag are converged after only two to four multigrid cycles on each grid.

A second case for the Kármán-Trefftz airfoil at the same freestream Mach number but an angle-of-attack of 10° is shown in Figs 5 and 6. The comparison of surface pressures with exact values shows very good agreement. The 65×65 grid solution misses the suction peak

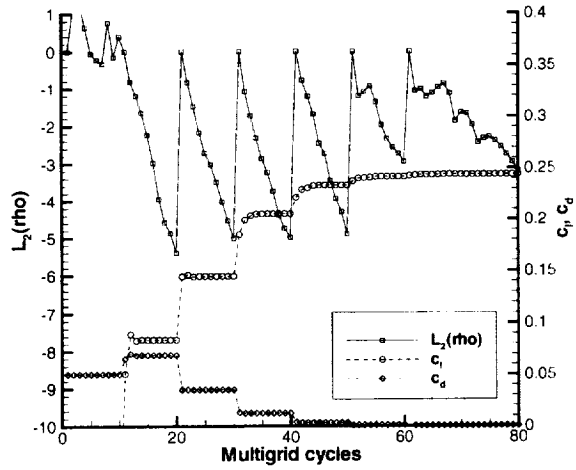

Figure 4. Convergence of residual and forces for a Kármán-Trefftz airfoil, $M_\infty = 0.01$, $\alpha = 2°$, finest grid 257×257 grid.

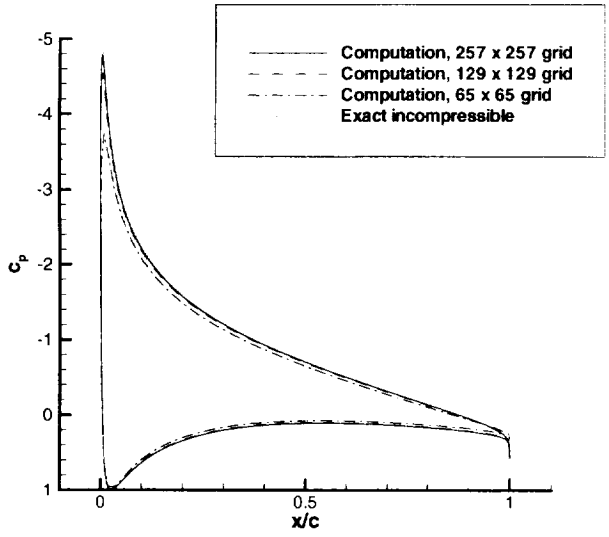

Figure 5. Surface C_p comparisons for a Kármán-Trefftz airfoil, $M_\infty = 0.01$, $\alpha = 10°$, finest grid 257×257 grid.

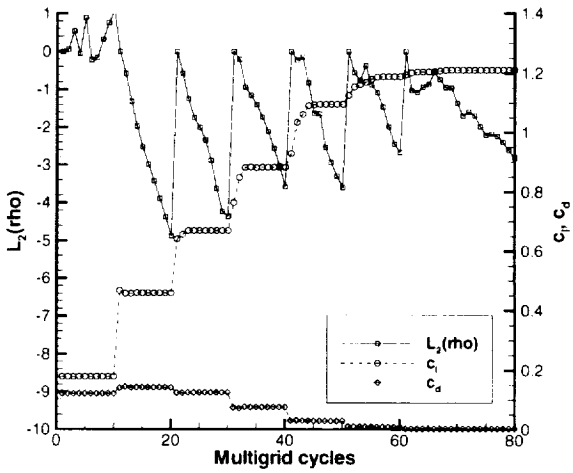

Figure 6. Convergence of residual and forces for a Kármán-Trefftz airfoil, $M_\infty = 0.01$, $\alpha = 10°$, finest grid 257×257 grid.

noticeably, but the two finest grid are very close to the analytic solution. The convergence rates shown in Fig. 6 are very similar to the previous case. The asymptotic rate for the continuity equation residual is about 0.35 per cycle on the coarser grids, and about 0.6 on the finest grid. The lift is converging more slowly on the finest grid, taking about five multigrid cycle to reach its asymptotic value.

A transonic case is shown next, with a freestream Mach number of 0.7 and an angle-of-attack of 1°. The surface C_p distribution is shown in Fig. 7, showing the upper-surface shock at approximately 30% chord. The peak Mach number on the airfoil is approximately 1.15. Convergence rates are shown in Fig. 8 and are comparable to the subsonic case. The forces are converging in about three to four cycles on each grid.

The grid for the cases shown above is orthogonal with unit aspect ratio cells. To ascertain how the scheme behaves in a more realistic case, subsonic and transonic solutions for a NACA 0012 have been obtained on an algebraically generated O-grid. The grid generator uses the transfinite interpolation method of Eriksson[8]. The grid near the airfoil is shown in Fig. 9. The fine-grid dimensions are 257×129 with the outer boundary located approximately 100 chords from the airfoil surface. The grid is more skewed at the trailing edge than the Kármán-Trefftz grid, and the cell aspect ratios vary from about 1:1 to 4:1. This grid is representative of a good-quality O-grid for a single-element airfoil. The coarsest grid is 9×5, and the same FMG cycle and boundary conditions are used as for the Kármán-Trefftz airfoil.

A solution for freestream Mach number of 0.01 and

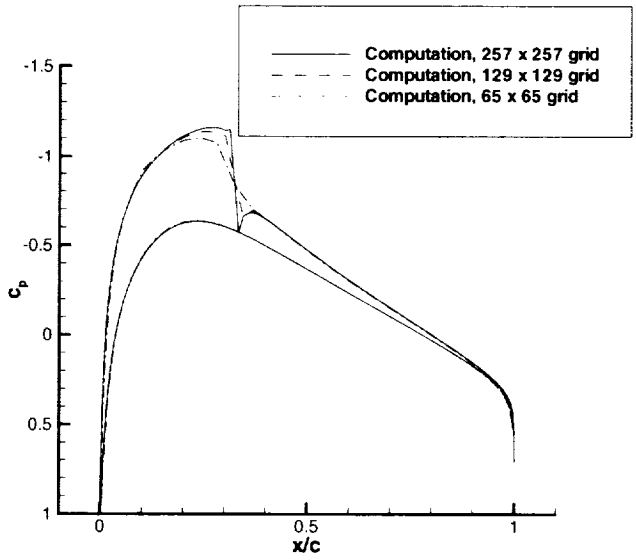

Figure 7. Surface C_p comparisons for a Kármán-Trefftz airfoil, $M_\infty = 0.70$, $\alpha = 1°$, finest grid 257×257 grid.

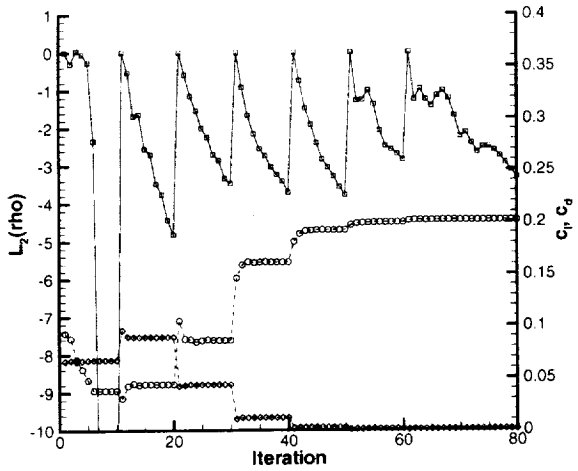

Figure 8. Convergence of residual and forces for a Kármán-Trefftz airfoil. $M_\infty = 0.70$, $\alpha = 1°$, finest grid 257×257 grid.

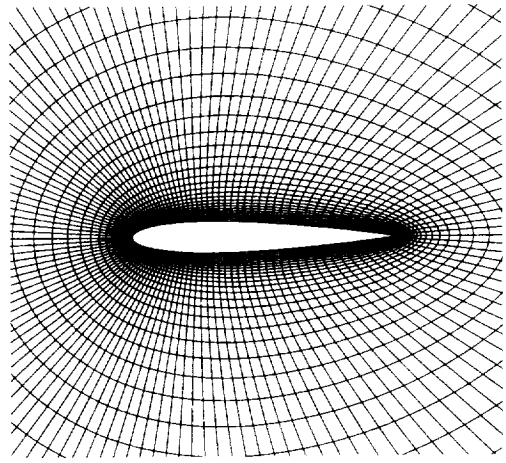

Figure 9. Algebraic grid for NACA 0012 airfoil.

angle-of-attack of 2° is shown in Fig. 10. Convergence rates are shown in Fig. 11. A deterioration in the convergence rates compared to the Kármán-Trefftz airfoil is observed, and the rate now appears to be slightly more grid-dependent. This is attributed to the varying aspect ratio of the grid cells. The asymptotic rate on the finest grid is about 0.5 per cycle. The forces are converging in about six to seven cycles on all grids.

The final results is for the standard test case of $M_\infty = 0.80$, $\alpha = 1.25°$. This is a much more severe transonic case than the one shown for the Kármán-Trefftz airfoil. The solution in Fig. 12 shows the strong suction-surface shock at about 60% chord, and the weak pressure-surface shock. The peak Mach number on the suction surface is about 1.35. The convergence rates for this case are shown in Fig. 13. The asymptotic rate for the continuity residual is quite slow on the finest grid, although the forces are converging in six to seven cycles.

A major part of the slowdown in the convergence rate stems from the anisotropy of the full-potential factor in the transonic regime. This was not as significant as for the Kármán-Trefftz result shown in Fig. 8 because of the relatively small size of the supersonic region in that case and the lower freestream Mach number. Point relaxation becomes decreasingly effective as a smoother for strongly supercritical flows. This can be alleviated by using line relaxation in the radial direction, which has the additional benefit of being more effective on stretched grids.

Conclusions

A factorizable discretization of the compressible Euler equations on general curvilinear body-fitted grids has been presented. This work is an extension of the previous results of Roberts, Sidilkover and Thomas to lifting airfoil flows. A modification of the original dissipation has been introduced to preserve the stability of the point collective Gauss-Seidel smoother without destroying the factorizability of the discretization A significant simplification of the original scheme has been the elimination of streamwise relaxation and replacing it with simple lexicographic symmetric relaxation. Both subsonic and transonic results for Kármán-Trefftz and NACA 0012 airfoils demonstrates good accuracy and fast convergence. Nearly $O(n)$ convergence rates for the residual are demonstrated subsonically and for slightly supercritical flows. The convergence for a more strongly transonic flow is significantly slower primarily because of the anisotropy of the differential operator in the transonic regime. The use of line relaxation should improve this, and additionally is should be well-suited for more severe grid stretching.

Acknowledgments

The author would like to thank his colleague David Sidilkover for his continual input of experience and suggestions, and for many clarifying discussions regarding the properties of his scheme. The author also gratefully acknowledges the technical discussions with and support of Jim Thomas and Charlie Swanson.

References

1. Roberts, T. W., Swanson, R. C., and Sidilkover, D., "An Algorithm for Ideal Multigrid Convergence for the Steady Euler Equations," *Computers and Fluids*, vol. 28, nos. 4–5, pp. 427–442, 1999.

2. Thomas, J. L., Diskin, B., and Brandt, A., "Distributed Relaxation Multigrid and Defect Correc-

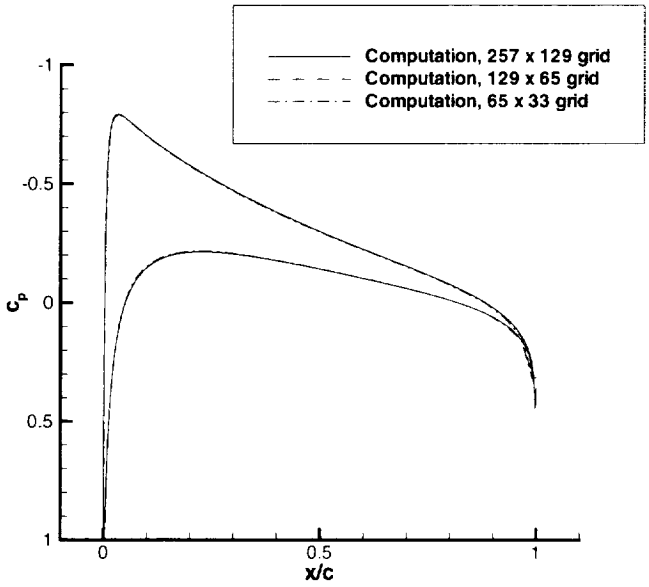

Figure 10. Computed surface C_p for a NACA 0012 airfoil, $M_\infty = 0.01$, $\alpha = 2°$, finest grid 257×129 grid.

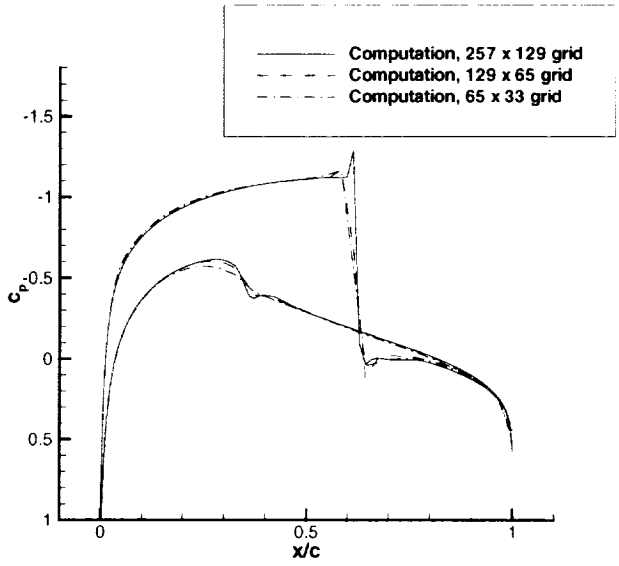

Figure 12. Computed surface C_p for a NACA 0012 airfoil, $M_\infty = 0.80$, $\alpha = 1.25°$, finest grid 257×129 grid.

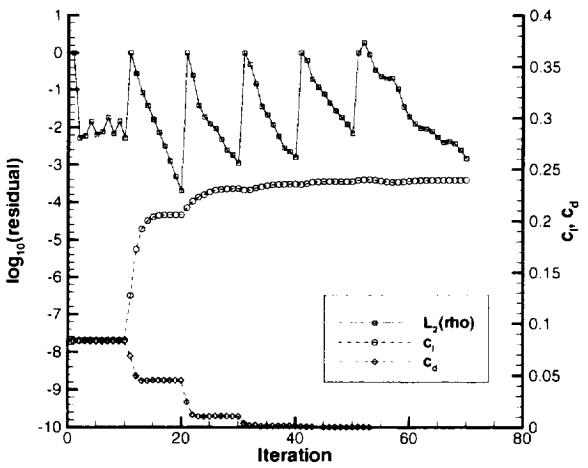

Figure 11. Convergence of residual and forces for a NACA 0012 airfoil, $M_\infty = 0.01$, $\alpha = 2°$, finest grid 257×129 grid.

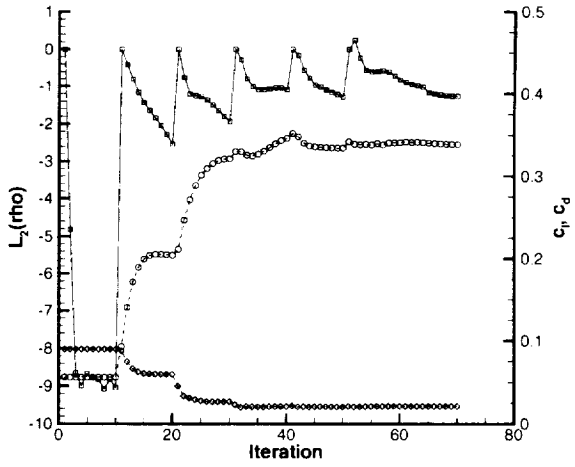

Figure 13. Convergence of residual and forces for a NACA 0012 airfoil, $M_\infty = 0.85$, $\alpha = 1.25°$, finest grid 257×129 grid.

tion Applied to the Compressible Navier-Stokes Equations," *AIAA Paper* 99-3334, 1999.

3. Roberts, T. W., Sidilkover, D., and Thomas, J. L., "Multigrid Relaxation of a Factorizable, Conservative Discretization of the Compressible Flow Equations," *AIAA Paper* 00-2252, 2000.

4. Brandt, A., "Multigrid Techniques: 1984 Guide with Applications to Fluid Dynamics," GMD-Studie 85, GMD-FIT, 1985.

5. Sidilkover, D., "Factorizable Schemes for the Equations of Fluid Flow," ICASE Report 99-20, 1999.

6. Sidilkover, D., "A Genuinely Multidimensional Upwind Scheme and Efficient Multigrid Solver for the Compressible Euler Equations," ICASE Report 94-84, 1994.

7. Giles, M., "UNSFLOW: A Numerical Method of Unsteady Inviscid Flow in Turbomachinery," GTL Report 195, Massachusetts Institute of Technology Gas Turbine Laboratory, October 1988.

8. Eriksson, L.-E., "Generation of Boundary-Conforming Grids Around Wing-Body Configurations Using Transfinite Interpolation," *AIAA Journal*, vol. 20, no. 20, pp. 1313-1320, October 1982.